SIMULTANEOUS DETERMINATION OF THE TWO-PHASE FLOW AND HYDRODYNAMIC DISPERSION COEFFICIENTS OF SOILS FROM TRANSIENT IMMISCIBLE AND MISCIBLE DISPLACEMENT EXPERIMENTS

Christos Aggelopoulos[1,2], Christos D. Tsakiroglou[1,*]

[1]FORTH / ICE-HT, Stadiou Street, Platani, P.O. Box 1414, GR – 26504 Patras, Greece
[2]Department of Physics, University of Patras, GR – 26504 Patras, Greece

This paper was prepared for presentation at the International Symposium of the Society of Core Analysts held in Toronto, Canada, 21-25 August 2005

ABSTRACT

A method is described to determine the relative permeability curves, capillary pressure curve and longitudinal dispersion coefficient of disturbed soils by monitoring multi-point measurements of the electrical resistance during transient immiscible and miscible displacement experiments. The electrical measurements are employed to calculate the transient response of the average water saturation over various segments of the soil, and solute concentration breakthrough curve at various axial positions of the soil. The experimental datasets are introduced into numerical codes of inverse modeling of the two-phase flow and advection-dispersion equations to estimate the relative permeability curves, the capillary pressure curve, and the longitudinal dispersion coefficient.

INTRODUCTION

The capillary pressure and relative permeability curves may be determined by performing either steady-state experiments with the simultaneous flow of both fluids through the porous medium [1] or transient experiments of the displacement of the one fluid by the other [2]. Albeit accurate, the steady-state methods are expensive and time-consuming. The transient experiments are fast and the two-phase flow coefficients are estimated implicitly by using the macroscopic two-phase flow equations, with history matching of the transient evolution of the pressure drop and spatial distribution of the fluid saturation [3,4]. The hydrodynamic dispersion coefficients are commonly estimated from datasets of miscible displacement experiments by fitting analytic or numerical solutions of the advection-dispersion equation to the transient variation of the solute concentration [4-6].

In the present work, immiscible and miscible displacement experiments are performed on disturbed soil columns, and the electrical resistances measured between vertical ring

* Corresponding author, e-mail: ctsakir@iceht.forth.gr, Tel.: 2610 965212, Fax: 2610 965223

electrodes and horizontal rod electrodes are converted to transient responses of water saturation and solute concentration. Numerical codes of inverse modeling of the two-phase flow and advection-dispersion equations are employed to estimate the capillary pressure curve, the relative permeability curves, and the longitudinal dispersion coefficient.

METHODS AND MATERIALS

The porous medium consists of sieved sand with grain size distribution in the range 125-250 μm, porosity $\varepsilon = 0.4$, and permeability $k = 35.8$ Da [7]. The experimental apparatus (Fig.1a) includes a PTFE holder equipped with two end electrodes and intermediate ring electrodes (Fig.1b), a hand-made multi-point conductivity meter, a syringe pump, a weight balance, a differential pressure transducer, and a pressure indicator. Two PTFE holders were used: a large one with length $L = 30$ cm and diameter $D = 5$ cm, and a small one with $L = 13.7$ cm and $D = 3$ cm.

During an immiscible displacement experiment, the oil phase (n-dodecane) is injected steadily at a constant and relatively low influx rate (q=0.1 ml/min) until steady-state conditions are established. Afterwards, the flow rate increases (q=0.5 ml/min) and the electrical resistance across the various sand segments (Fig.1b), effluent weight, and total pressure drop are monitored until a new steady-state is reached.

During a miscible displacement experiment, the sand is filled with a low NaCl concentration ($C_i = 17.1$ mol/m^3) solution, whereas a high NaCl concentration ($C_0 = 68.4$ mol/m^3) solution is injected at a constant flow rate upwards. The transient response of the electrical resistance between each pair of the rod electrodes (Fig.1c) is measured and then is transformed to the solute concentration breakthrough curve by using the corresponding calibration curve.

RESULTS AND DISCUSSION

Immiscible displacement experiments

The capillary pressure and relative permeability curves were estimated from vertical displacement experiments performed on the small sand column at capillary number $Ca = 6.2\text{x}10^{-8}$ and $Ca = 3.1\text{x}10^{-7}$. The transient response of the total pressure drop across the column (Fig.2a) increases abruptly as the displacing oil phase penetrates in the porous medium and the capillary resistance is added in the viscous pressure drop. As the pore size distribution is narrow, and the viscosity ratio is not far from unity ($\kappa = 1.42$) , the pre-breakthrough $\Delta P(t)$ remains almost constant, whereas the post-breakthrough $\Delta P(t)$ falls sharply and remains constant up to the moment that the flow rate increases and $\Delta P(t)$ increases again (Fig.2a). The capillary number is low, the density difference is negative ($\rho_o - \rho_w < 0$), and subsequently the displacement is governed by capillary fingering at the pore network-scale but it is a stable frontal drive at the macroscopic scale of the column [7]. The electrical resistance is measured in three cumulative segments of

the column (1-2, 1-3, 1-4 in Fig.1a) whereas the corresponding water saturation is calculated easily from the volume injected and the weight of the effluents. From the measurements of the resistivity index and water saturation in each cumulative segment, the parameters of the following relationship are estimated with non-linear fitting

$$I_R = \left[a {S_w}^m + (1-a) {S_w}^l \right]^{-1} \tag{1}$$

where the exponent m is dominant over high and intermediate water saturations with heterogeneous fluid distribution along the sand column, and the exponent l is dominant over low water saturations with the fluid distribution tending to be homogenized [7]. From the measured cumulative resistivity index curves of the segments 1-2, 1-3, 1-4, the total pore volume of each segment, V_{ij}, and simple mass balances of the form

$$S_{w1-3} = \left(S_{w1-2} V_{p12} + S_{w2-3} V_{p23} \right) / V_{13} \tag{2}$$

we get the water saturation ($S_{w1-2}, S_{w2-3}, S_{w3-4}$) of each differential segment of the column (Fig.2b).

The steady-state axial water saturation distribution along the sand column is not uniform but increases in the deeper layers of the column (Fig.2b). This is due to the capillary end effect which is associated with the discontinuity of the capillary pressure at the outlet of the porous medium and affects significantly the estimated relative permeabilities [8,9].

The unsteady two-phase flow in porous media is described by a mixed system of PDE and algebraic equations which is solved numerically along with the adequate initial and boundary conditions [3,4]. The $k_{rw}(S_w), k_{ro}(S_w), P_c(S_w)$ are so selected that the numerically calculated responses of $\Delta P(t)$ and $S_{wi-j}(t)$ fit to the corresponding experimental measurements (Figs.2a,b). The inverse modeling was done by using the Baeysian estimator and Gregplus PDE solver of Athena Visual Studio 10.0 [3,4] and preliminary results are shown in Fig.3a,b. The width of the $P_c(S_w)$ is small in agreement with the narrow pore size distribution of the sand (Fig.3a). The $k_{rw}(S_w)$ and $k_{ro}(S_w)$ are non-linear and quasi-linear function of S_w, respectively (Fig.3b), in qualitative agreement with analogous results obtained from experiments performed on planar porous media [3].

During an immiscible displacement at a finite flow rate, the fluid saturation varies respectably across a fractal frontal region [3,4]. The $P_c(S_w)$, $k_{rw}(S_w)$ and $k_{ro}(S_w)$ depend on the spatial distribution of the two phases within this region as a result of the interactions of the pore structure, viscous forces and buoyancy forces. In a drainage experiment performed at low Ca values, the thickness of the frontal region, dominated by capillary fingering, is quite wide compared to the sample length [3]. In this 3-D case, the density difference $\Delta\rho = \rho_o - \rho_w < 0$, and buoyancy forces stabilize the displacement front [7]. An analogous stabilization of the displacement front in a planar (2-D) porous medium (glass-etched pore network) is described in [3] where an axial gradient of the capillary pressure caused by the viscous forces results in $k_{rw}(S_w)$ and $k_{ro}(S_w)$ which

are increasing functions of Ca. Subsequently, the $k_{rw}(S_w)$ and $k_{ro}(S_w)$ of the sandpack are expected to be decreasing functions of the Bond number, B, defined by $\mathrm{B} = \Delta\rho g_z \langle r_t \rangle \langle D_g \rangle / (2\gamma \cos\theta)$ (g_z = vertical component of gravity vector, $\langle r_t \rangle$ = mean throat radius, $\langle D_g \rangle$ = mean grain diameter, γ = interfacial tension, θ = contact angle) [7]. On the other hand, the sensitivity of $P_c(S_w)$, $k_{rw}(S_w)$ and $k_{ro}(S_w)$ to Ca may be weak for 3-D media compared to 2-D ones, because of the coexistence of two phases across the porous medium (bi-continua) over a wide range of fluid saturations. The classical invasion percolation model is unable to explain the fluid distribution across the porous medium as well as the variation of P_c, k_{rw}, k_{ro} with B, Ca. Instead, a gradient percolation model could be used to predict such a behavior [3]. The long-term objective of the present work is to combine fundamental knowledge of the 2-phase flow in porous media, such as the gradient percolation theory, with the conventional macroscopic approach in order to quantify the effects of capillary number and Bond number on P_c, k_{rw}, k_{ro} of soils.

Miscible displacement experiments

The longitudinal dispersion coefficient was estimated from miscible displacement experiments performed on the large sand column at low values of the Peclet number (Pe=0.5-25) defined by

$$Pe = u_{p0} \langle D_g \rangle / D_m \qquad (3)$$

where $u_{p0} = Q/(\varepsilon A)$ is the pore velocity, $\langle D_g \rangle$=200 μm, and D_m is NaCl-H_2O bulk diffusion coefficient ($D_m = 1.6x10^{-9}$ m^2/s). The solute concentration breakthrough curves measured at three distances from the column inlet are shown in Fig.4. The transient response of the solute concentration at distance x from the column inlet is described by the analytic solution of the one-dimensional advection-dispersion equation [4-6]. With the aid of the Athena Visual Studio 10.0, experimental breakthrough curves were fitted with this analytic solution to estimate simultaneously, the pore velocity, u_{p0} and longitudinal dispersion coefficient, D_L. Although, almost identical and reliable "average" values of u_{p0} were estimated from the three breakthrough solute concentration curves, the D_L values were overestimated (Fig.4). The solution is injected in the porous medium through a hole of the end electrode (Fig.1a,b). The continuity equation coupled with Darcy equation was solved analytically in a cylindrical homogeneous porous medium, where a uniform flow velocity profile is implied over a small circular area around the axis of the cylinder. It was found that the flow field becomes fully developed at a short distance from the column inlet, which means that the assumption of 1-D flow of constant velocity throughout the porous medium was not far from reality. The overestimated D_L value (Fig.4) might be attributed to the deviation of the solute concentration field from the uniform profile at the column inlet, and the necessity of

using the 1-D advection / 2-D dispersion equation with a solute flux boundary condition, including the transverse dispersion coefficient, D_T, to describe the solute-transfer in the soil.

ACKNOWLEDGEMENTS

This work was performed under Global Change and Ecosystems contract number SSPI-CT-2003-004017-STRESOIL (2004-2007) supported by the European Commission.

REFERENCES

1. Avraam, D.G. and A.C. Payatakes, "Flow regimes and relative permeabilities during steady-state two-phase flow in porous media" *J. Fluid Mech.*, (1995) **293**, 207-236.
2. Chen, J., J.W. Hopmans, and M.E. Grismer, "Parameter estimation of two-fluid capillary pressure-saturation and permeability functions", *Adv. Water Resour.*, (1999) **22**, 479-493.
3. Tsakiroglou, C.D., M. Theodoropoulou, and V. Karoutsos, "Non-equilibrium capillary pressure and relative permeability curves of porous media", *AIChE J.*, (2003) **49,** 2472-2486.
4. Tsakiroglou, C.D., M.A. Theodoropoulou, V. Karoutsos, and D. Papanicolaou, "Determination of the effective transport coefficients of pore networks from transient immiscible and miscible displacement experiments", *Water Resources Research*, (2005) **41(2)**, W02014.
5. Inoue, M., J. Simunek, S. Shiozawa, J.W. Hopmans, "Simultaneous estimation of soil hydraulic and solute transport parameters from transient infiltration experiments", *Adv. Water Resour.*, (2000) 23, 677-688.
6. Sahimi M., "Flow and Transport in Porous Media and Fractured Rock**:** From Classical Methods to Modern Approaches", (1995) VCH, Weinheim, Germany.
7. Aggelopoulos, C., P. Klepetsanis, M. Theodoropoulou, K. Pomoni, and C.D. Tsakiroglou, "Large-scale effects on the resistivity index of porous media", *J. Contam. Hydrology*, (2005) **77,** 299-323.
8. Huang, D.D. and M.M. Honarpour, "Capillary end effects in coreflood calculations", *J. Pet. Sci. Eng.*, (1998) **19**, 103-117.
9. Toth, J., T. Bodi, P. Szucs and F. Civan, "Convenient formulae for determination of relative permeability from unsteady-state fluid displacements in core plugs", *J. Pet. Sci. Eng.*, (2002) **36**, 33-44.

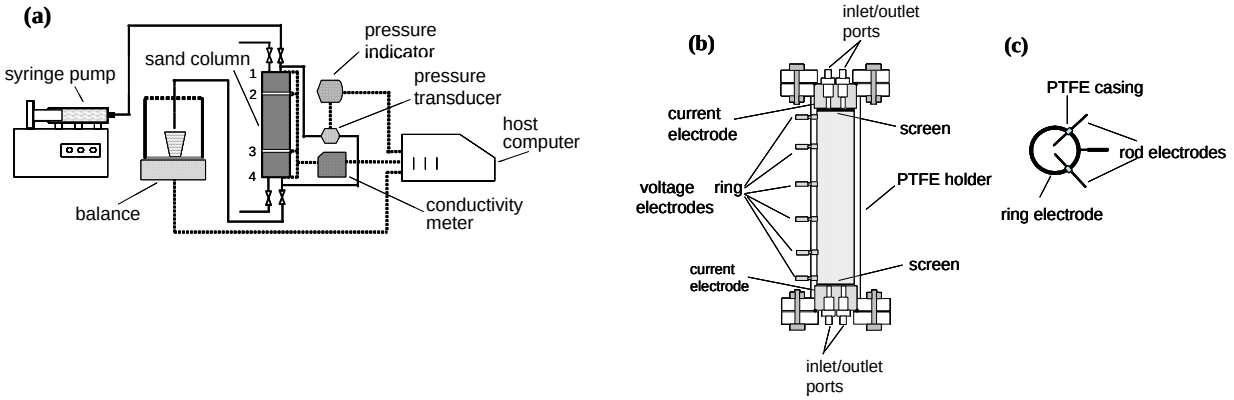

Figure 1. (a) Setup for performing immiscible displacement on the small resistivity cell; the displacement is downwards. (b) Schematic diagram of the large resistivity cell. (c) Overview of rod electrodes.

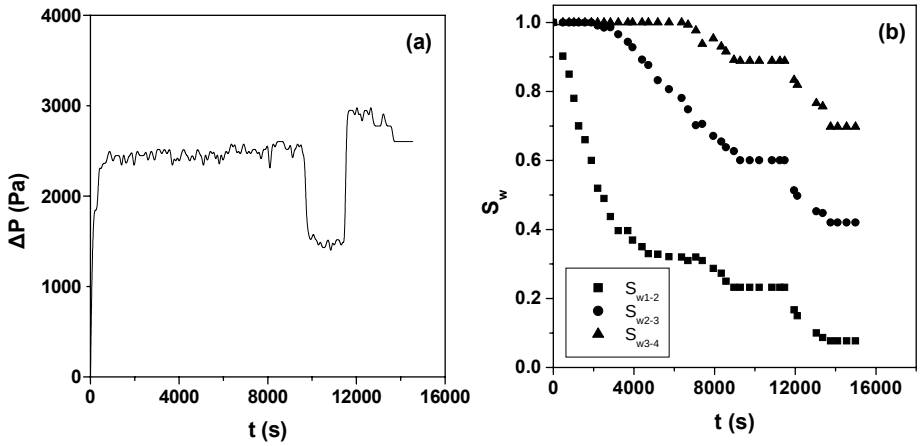

Figure 2. (a) Transient response of the pressure drop across the small sand column. (b) Transient response of the water saturation for the column segments 1-2, 2-3, 3-4.

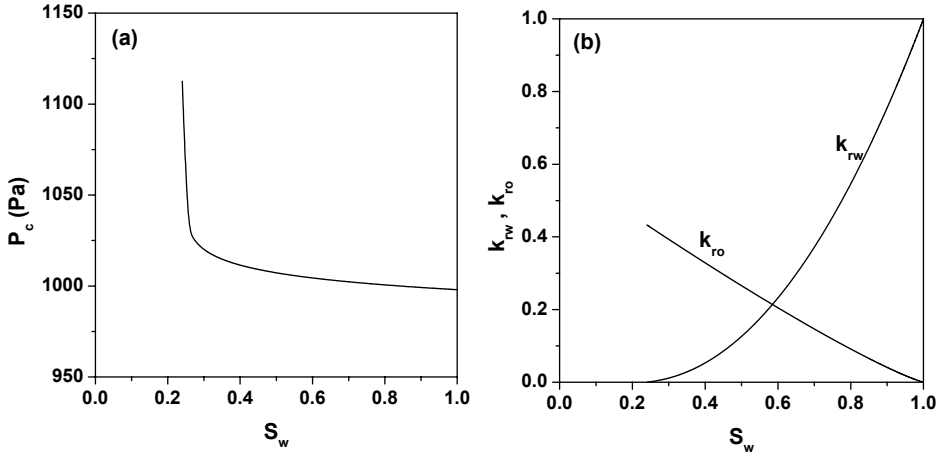

Figure 3. (a) Estimated capillary pressure curve. (b) Estimated water and oil relative permeability curves.

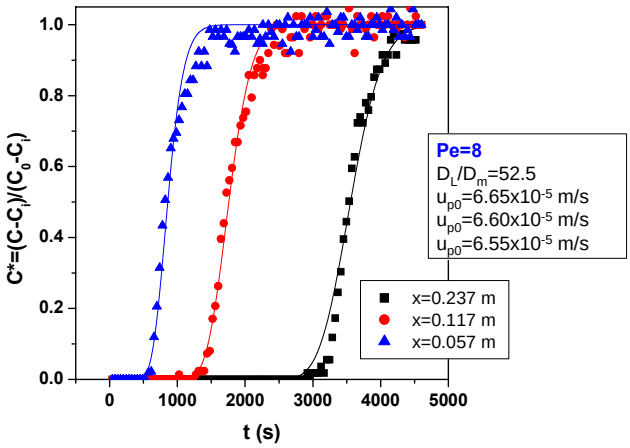

Figure 4. Experimentally measured vs. numerically predicted solute concentration breakthrough curves.